Bulk Lifetimes up to 20 ms Measured on Unpassivated Silicon Discs Using Photoluminescence Imaging

Daniel Chung, Bernhard Mitchell, Mohsen Goodarzi, Chang Sun, Daniel Macdonald, and Thorsten Trupke

***Abstract*—With high-efficiency silicon solar cells approaching 25% efficiency in mass production, the requirements on the bulk lifetime and its uniformity across the wafer and the ingot increase dramatically. Since some cell architectures require these high lifetimes on starting material, the need arises for characterization methods to measure very high bulk lifetimes that are spatially resolved at an early stage before cell processing. A method based on the spectral ratio of two photoluminescence images is applied here on two unpassivated silicon discs from different positions within a Czochralski-grown phosphorous-doped n-type silicon ingot. The method allows the determination of spatially resolved bulk lifetime images on samples with adequate thickness and can be done within seconds and without the need to passivate surfaces. As-grown bulk lifetimes up to 20 ms are measured on the ingot's central disc, indicating recent improvements in crystallization technology, but are strongly reduced closer to the crown. Evidence suggesting the impact of thermal donors on the lifetime and effective doping concentration near the crown is found from combining spectral photoluminescence and infrared spectroscopy analyses. The technique could find applications in research and development activities, particularly in the optimization of Czochralski silicon crystal growth conditions.**

***Index Terms*—Charge carrier lifetime, imaging, photoluminescence (PL), silicon (Si).**

I. Introduction

LARGE-SCALE production of monocrystalline silicon (Si) for the photovoltaics (PVs) industry is predominantly through the Czochralski (CZ) growth process. Although n-type phosphorous-doped CZ-Si is capable of minority carrier bulk lifetimes exceeding several milliseconds, the CZ process is not immune to recombination active defects, particularly oxygen precipitates [1] and the related thermal donors (TD) [2]. High-efficiency solar cells such as the Si heterojunction (SHJ) cell [3] and the interdigitated back contact (IBC) [4] cell require multimillisecond as-grown bulk lifetimes in order to achieve the high efficiencies that are reported in the literature. Here, we utilize a fast photoluminescence (PL) imaging method for measuring bulk lifetime on thick, unpassivated Si discs to support research and development activities aimed at understanding the interactions between crystal growth, material quality, and the efficiency of solar cells made using architectures such as SHJ and IBC. Two samples originating from the same ingot, cut in the wafer plane, are studied using this technique.

On the ingot level, prior to wafering, bulk lifetime can be accessed through measurements on the bricks' side faces, for example through photoconductance [5] (PC) or PL methods [6], [7]. With sense depths in the order of a few millimeters [5], [6], the resulting bulk lifetime data represents only the perimeter of wafers cut from these bricks. Significant variations in lifetime can occur in the radial direction from the central axis of the ingot toward the side faces. After the cylindrical ingots are trimmed into pseudo-square bricks, these internal lifetime variations may be seen in brick measurement depending on how far the defects extend toward the perimeter. However, to spatially resolve all the lifetime variations inside an ingot, measurements should be done after wafering. The difficulty with bulk lifetime measurements on thin as-cut wafers is that the measured lifetime is dominated by surface recombination. Additional processing is, therefore, required for surface passivation, and extremely small surface recombination velocities would be needed to resolve lifetimes in the 20 ms range. Grant *et al.* [8] show that temporary liquid HF passivation is a fast and effective treatment for this purpose; however, HF concentration, exposure to light, and trapping artifacts can affect the measurement results. To overcome the limitations in both approaches and to gain a reliable measure of the CZ ingots' bulk quality, we utilize spectral PL imaging under quasi-steady-state conditions on thick unpassivated Si discs cut in the wafer plane.

II. Theory and Modeling

For polished Si samples, the relative spectral PL intensity can be described in a 1-D model as

$$\mathrm{PL}(\lambda) \propto \int_0^w B(\lambda)\, n(x,\tau_b)\; p(x,\tau_b)\; f_{\mathrm{esc}}(\lambda,x)\; dx \quad (1)$$

Manuscript received October 5, 2016; accepted December 19, 2016. Date of publication January 9, 2017; date of current version February 16, 2017. This work was supported by the Australian Renewable Energy Agency under Grant 7-F008 and Grant RND009. Responsibility for the views, information, or advice expressed herein is not accepted by the Australian Government.

D. Chung and B. Mitchell are with the Australian Centre for Advanced Photovoltaics and the School of Photovoltaic and Renewable Energy Engineering, University of New South Wales, Kensington, N.S.W. 2052, Australia (e-mail: daniel.chung@unsw.edu.au; bernhard.mitchell@unsw.edu.au).

M. Goodarzi, C. Sun, and D. Macdonald are with the Research School of Engineering, Australian National University, Canberra, A.C.T. 2601, Australia (e-mail: mohsen.goodarzi@anu.edu.au; chang.sun@anu.edu.au; daniel.macdonald@anu.edu.au).

T. Trupke is with the Australian Centre for Advanced Photovoltaics and the School of Photovoltaic and Renewable Energy Engineering, University of New South Wales, Kensington, N.S.W. 2052, Australia, and also with BT Imaging Pty Ltd., Waterloo, N.S.W. 2017, Australia (e-mail: t.trupke@unsw.edu.au).

Color versions of one or more of the figures in this paper are available online at http://ieeexplore.ieee.org.

Digital Object Identifier 10.1109/JPHOTOV.2016.2644984

where $B(\lambda)$ is a spectrally dependent radiative recombination coefficient [9], $n(x, \tau_b)$ and $p(\mathrm{x}, \tau_b)$ are the electron and hole concentrations at depth x in material with bulk lifetime τ_b, f_{esc} is the photon escape probability, and w is the sample thickness. In this measurement, excess electrons and holes are generated relatively close to the surface using a laser. With increasing bulk lifetime and thus longer diffusion length, the charge carriers diffuse deeper into the material resulting in a relative decrease in short wavelength luminescence [6]. These relative spectral changes in PL emission can be used to find bulk lifetime rather than using absolute measurements of PL and fitting to (1). PL spectral changes are measured using PL intensity ratios (PLIRs) as described by Mitchell *et al*. [6]. PLIR is the ratio of two PL images that are measured with different spectral filters in front of the detection system and is given by

$$\mathrm{PLIR} = \frac{\int T_{\mathrm{LP}}(\lambda)\,\mathrm{QE}(\lambda)\,\mathrm{PL}(\lambda)\,d\lambda}{\int T_{\mathrm{SP}}(\lambda)\,\mathrm{QE}(\lambda)\,\mathrm{PL}(\lambda)\,d\lambda} \tag{2}$$

where T_{LP} and T_{SP} are the spectral transmissions of the long pass and short pass filters, respectively, used in the two PL images and QE is the camera's quantum efficiency. Apart from the spectral filters, the two PL images are taken under the same measurement conditions, which simplifies calibration since many depth and spectrally independent terms cancel out in the ratio. These include laser intensity and sample doping if measurements are taken under low injection conditions.

A number of assumptions included in previous PLIR applications on Si bricks (effectively infinitely thick samples) are not valid for thinner samples. When the thickness of the sample is not sufficiently larger than the diffusion length, the electron and hole concentrations in (1) are influenced by both the rear and front surface leading to a different PL emission, as provided by Green [10]. We use a modified version of the numerical modeling tool PC1D [11] to model electron and hole concentrations. The simulation is set up with a single region with appropriate doping, thickness, and planar surfaces. Front and rear surfaces are assumed to have a surface recombination velocity of 2×10^5 cm/s [7], although the precise value for this sample is not known. If the surface recombination is any value above 10^5 cm/s, the resulting uncertainty in the calculated bulk lifetime is a minor $\pm 2\%$ for the surface recombination value assumed. Where a choice of model is available in PC1D, we used "Schenk" bandgap narrowing [12], "Klaassen" carrier mobility [13], [14], "Richter" intrinsic recombination [15], and all the remaining model options were kept to the updated defaults which have been tabulated in detail by Haug *et al.* [11]. The bulk lifetime in PC1D can be varied using a single Shockley–Reid–Hall defect. We varied "tau-p" and set "tau-n" and defect energy level to 0 for n-type samples. Since Auger and radiative recombination are also included in the simulation, the resulting bulk lifetime can be found by a virtual lifetime measurement of the sample by calculating the ratio of total minority carrier concentration and total generation rate in the sample when surface recombination is set to 0 and the light intensity is reduced to match the weighted average injection [16] for the case with 2×10^5 cm/ s surface recombination. In Fig. 1, we show examples of the normalized hole concentration profiles calculated by PC1D for a variety of lifetimes, material thicknesses, and surface recombination velocities.

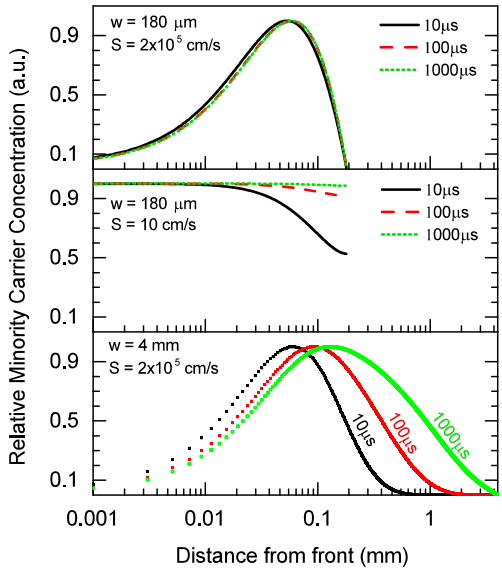

Fig. 1. Simulated minority carrier concentration profiles normalized to the maximum value for 180 μm samples with and without surface passivation and a 4 mm thick sample without surface passivation. Note that each frame contains the width (w) and surface recombination velocity (S) used in simulation. Each trace is labeled with the bulk lifetime simulated in microseconds. The samples are illuminated with a 900 nm excitation source at 0.001 W/cm^2 and have n-type doping of 10^{15} cm^{-3} concentration.

PL detected by a camera must first travel a distance "x" through the sample and escape from the surface. Since it is possible that PL emission is re-absorbed by the Si on the way to the surface, the escape probability can be less than 1. In thin samples, the photon escape probability [9] is given as follows, which takes into account multiple internal reflections

$$f_{\mathrm{esc}}(\lambda, x) = (1 - R_f)\,\frac{\exp(-\alpha x) + R_b \exp(-\alpha(2w - x))}{1 - R_f R_b \exp(-\alpha w)} \tag{3}$$

where α is the wavelength-dependent total absorption coefficient of Si, w is the sample thickness, and R_f and R_b are the spectral reflectance's of the front and rear surfaces, respectively. For the 4 mm sample in Fig. 1, increasing the bulk lifetime produces progressively deeper minority carrier profiles which cause spectral changes in PL emission in the same way that occurs in bricks [6]. However, for 180 μm in Fig. 1, there is minimal change in the depth profiles of minority carriers toward higher lifetimes, even when surface passivation is present. Surface passivation produces approximately uniform charge carrier profiles with depth and any changes in bulk lifetime only increase/decrease the overall concentration. This behavior would not produce spectral changes in PL emission detectable by PLIR measurements.

Fig. 2 shows PLIR transfer functions, i.e., the PLIR as a function of bulk lifetime for polished, Si of different thicknesses. At each bulk lifetime on the x-axis, the PLIR value is found by the numerical integration of (3) taking $n(x)$ and $p(x)$ from PC1D through the command line interface. A saturation in the

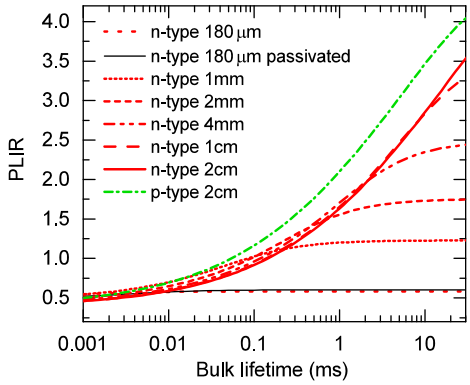

Fig. 2. Numerically simulated PLIR to bulk lifetime transfer functions. Values are modeled for the experimental system used in this work. Transfer functions are plotted for different sample thicknesses with surface recombination velocities at the front and rear set to 2×10^5 cm/s, except for the simulation "n-type 180 μm passivated," which has surface recombination velocity of 10 cm/s to indicate a typical surface passivated wafer. All data are modeled for a resistivity of 4.5 Ω cm under low injection conditions.

transfer function occurs toward high lifetimes, with the onset occurring at lower lifetime for thinner samples. It shows that for a wafer thickness of 180 μm, as is commonly used for PV, the PLIR contains virtually no information about the bulk quality for bulk lifetimes exceeding $\sim$10 μs, a fundamental physical limitation of lifetime measurements [17], [18]. This saturation is evident by examining the very similar relative minority carrier depth profiles in Fig. 1 for the 180 μm thick samples. Similarly, lifetimes above $\sim$ 150 μs would not be measurable on n-type wafers of standard thickness used in the electronics industry ($\sim$ 750 μm or less). Based on Fig. 2, a sample thickness exceeding 4 mm is required to differentiate lifetimes above 10 ms using the PLIR method. We note that p-type Si has a similar transfer function to n-type, as shown in Fig. 2 for the 2 cm thick sample. Since the PLIR is influenced by the diffusion length of carriers rather than the lifetime, n-type and p-type transfer functions are shifted by a scaling factor on the x-axis, which reflects the mobility ratio between electrons and holes, i.e., the same excess minority carrier diffusion length is achieved in p-type for lower bulk lifetime due to the higher electron mobility.

The transfer functions have a significant thickness dependence for samples $<$ 1 cm at higher bulk lifetimes. However, for the samples used in this study, small variations in the thickness of $\pm$1 mm cause $<$ 1% error in reported bulk lifetimes in the 1–20 ms range. Additionally, at low lifetimes, a less-significant thickness dependence arises due to the influence on the escape probability term in (1) primarily from rear surface reflections.

III. Experiment

Two samples of 17 cm diameter from the same CZ n-type ingot were examined. These samples were lapped to a uniform thickness within 1 mm across the disc and polished manually with a cloth polishing pad and a 1 μm diamond polishing suspension resulting in a mirror-like appearance. Such surface preparation minimizes the influence of nonuniformities and dead layers at the front surface for highest precision measurements but may not be necessary in routine measurements or when using a calibration standard. Key sample parameters are summarized in Table I.

TABLE I
Specifications of Samples Measured in This Study

Sample	Distance from seed	Thickness	Measured Doping
N80	80 mm	18.5 mm	1.9×10^{15} cm^{-3}
N674	674 mm	20.0 mm	1.1×10^{15} cm^{-3}

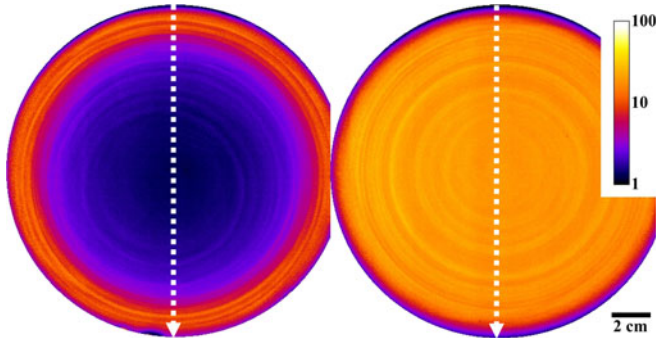

Fig. 3. Bulk lifetime images of sample N80 (left) and N674 (right). The color scale represents bulk lifetime in milliseconds and is mapped to lifetime logarithmically. Dotted lines represent the position of the cross-sections. Note that the samples are slightly larger than the field of view of the PL system.

Measurements were performed using a line scanning PL imaging system described in detail elsewhere [19]. Illumination was from an 880 nm diode laser with an adjustable intensity of 0.1 $-$ 2 W/ cm^2. The system includes a Si line scan camera and long-pass and short-pass filters with 1080 and 1030 nm cut-off wavelengths, respectively. Exposure times for unpassivated samples N80 and N674 were 3–20 s per image depending on illumination intensity and camera filtering. The spatial resolution of the PL images determined by the hardware in the system is 320 μm per pixel. The line-scan camera used in this measurement has been shown to significantly suppress the "point-spread" effect, even without deconvolution of the PL images, unlike typical Si area-scan cameras [19].

For comparison, each sample was measured using a Sinton BCT-400, which utilizes transient PC decay analysis and a 1/4+ flash setting. The same tool was used for dark resistivity measurements taken in the center of each sample.

IV. Results and Discussion

Bulk lifetime images for both samples are shown in Fig. 3 on the same logarithmic color scale. Sample N674 (shown on the right) is almost uniform with a median lifetime of 18 ms and peak lifetimes up to 20 ms, whereas N80 has one order of magnitude lower bulk lifetime in most regions of the disc, except for the edge region. Fig. 4 shows the corresponding bulk lifetime cross sections.

A number of spatial variations can be observed in the bulk lifetime images on both samples. Concentric rings are visible, most strongly in N674, which cause the peaks and troughs visible in

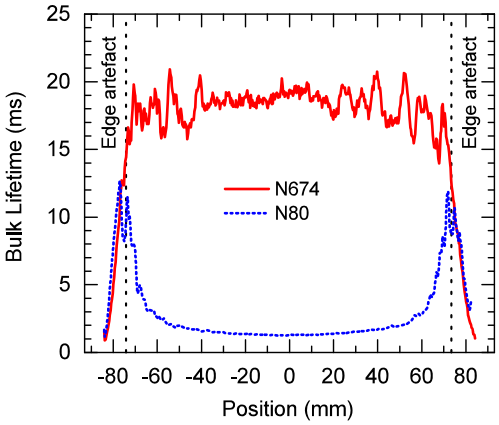

Fig. 4. Cross-sectional bulk lifetime profiles for samples N80 and N674. Vertical lines positioned toward the left and right edge of the cross-section indicate the measurement artefact caused by the surfaces toward the periphery of the discs.

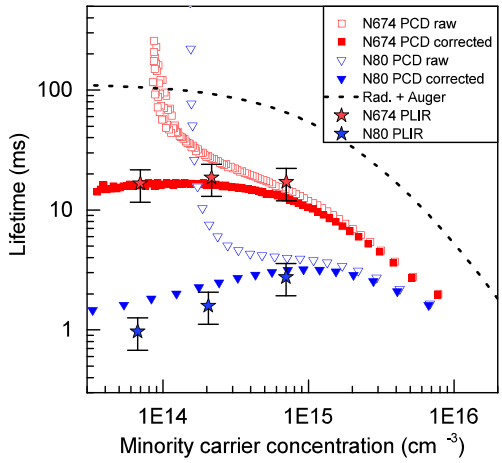

Fig. 5. Injection-dependent lifetime for samples N674 and N80 from transient photoconductance decay (PCD) measurements. Both raw data (open symbols) and trapping corrected data (solid symbols) are presented. Bulk lifetimes from PLIR are shown at three injection levels with errors bars based on an estimated uncertainty of the technique. The Auger and radiatively limited lifetime is also shown.

the cross section. The latter reveals amplitudes between 1 and 4 ms. These rings or striations have previously been observed in PL images on as-cut material with high interstitial oxygen concentrations [20]. Note that lateral and two-dimensional effects of carrier smearing are not included in the modeling of this study. Special cases of the carrier smearing have been quantified on multicrystalline Si bricks [21], but so far, no generalized quantitative analysis or desmearing algorithms [22] have been developed for thick samples with nonuniform carrier profiles. In general, the long carrier diffusion lengths found in the studied n-type Si result in more severe carrier smearing in thick wafer discs where the surfaces have less influence on carriers in the bulk. In fact, both samples are affected by an apparent reduction in bulk lifetime about 5–10 mm from the edge giving an indication of the carrier gradients introduced due to carrier smearing to a highly recombination active surface at the sides of the disc (labeled in Fig. 4 as an edge artefact).

The bulk lifetime values from PLIR were compared against the reported lifetime measured using transient PC decay (PCD) measurements. The raw PCD data plotted in Fig. 5 shows a strong increase in the reported lifetime toward low excess carrier densities to values exceeding the Auger and radiative lifetime limit, which is due to a minority carrier trapping artifact [23]. Similar trapping behavior in high quality n-type Si has been linked to the presence of TDs by Hu *et al.* [24], who also propose a trapping correction based on the subtraction of an offset in the raw conductance data, an approach which is also used here. Unlike PCD measurements, quasi-steady-state PL methods are not normally affected by trapping as long as the background doping is much larger than the trap density [25]. For the samples investigated here, we estimate the trap density to be up to $10^{14}\,\mathrm{cm}^{-3}$ based on the PC offset value in the transient PCD. Combined with doping of $\sim 10^{15}\,\mathrm{cm}^{-3}$, this ratio in trap to doping density would lead to a 10% overestimation of lifetime when using a single PL measurement [25]. However, since a spectral ratio of PL measurements is used in the PLIR method, uncertainty from trapping only arises if changes to the PL spectrum arise, i.e., from variations of the TD concentration with depth. It is unlikely that the TD concentration varies significantly with sample depth over the millimeter sense depth range of this measurement, so replacing the majority carrier concentration in (1) with $n(x) + n_t$ to account for the additional electrons arising from trapped holes has negligible influence on the PLIR.

PLIR measurements were performed at different laser intensities, resulting in bulk lifetime data at different average injection levels as defined by Bowden and Sinton [16]. Direct comparison of the PL and PCD techniques in Fig. 5 is difficult, but good agreement is observed in consideration of several artefacts. A low lifetime is reported by transient PCD for sample N674 at excess carrier densities above $10^{15}\,\mathrm{cm}^{-3}$, which is well below the intrinsic lifetime and apparent defect related lifetime of the sample. Swirhun *et al.* [5] have modeled transient PCD measurements for thick and unpassivated samples, which revealed that the reported lifetime is lower than the actual bulk lifetime at the early stage of the transient decay since charge carriers near the surface can recombine quickly. They also diffuse deeper into the sample out of the sensing range of the tool where they are predominantly generated. The reported lifetime only approaches the sample's actual bulk lifetime after the initial decay, i.e., when the carrier density has decreased by around two orders of magnitude [5, fig7]. This behavior is also strongly influenced by the duration of the flash in the measurement which should be longer than for typical transient measurements on wafers. We, therefore, attribute reduced lifetime reported from PCD in N674 and N80 above $10^{15}\,\mathrm{cm}^{-3}$ to that effect. In a separate discrepancy toward lower injections, PL measurements predict a lower lifetime than the PCD measurement for N80. This deviation is currently not well understood. Some possible explanations are the accuracy of the trap correction applied here which has not been thoroughly investigated for transient lifetime measurements on n-type Si and which increasingly affects injection levels below the trap concentration. Additionally, the evident injection

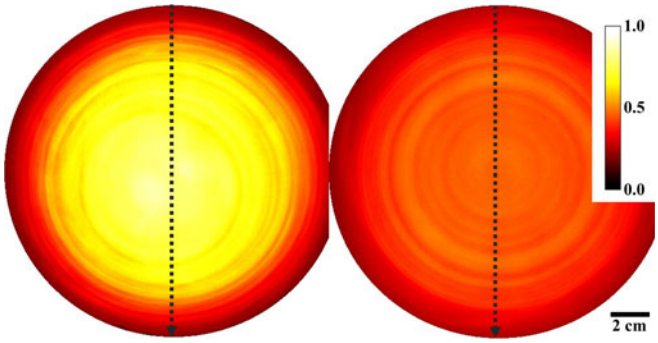

Fig. 6. Relative doping images calculated from bulk lifetime and PL counts for samples N80 (left) and N674 (right), both plotted on the same relative color scale. The dotted lines denote the positions of cross-section shown in Fig. 7.

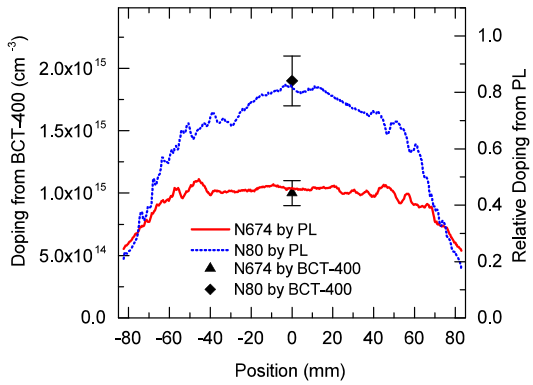

Fig. 7. Cross-sectional doping profiles for samples N80 and N674. The relative doping from PL is calibrated using the average of resistivity measurements from a Sinton Instruments BCT-400 in a central location on N80. Error bars for the BCT-400 measurements are based on repeated measurements.

dependence of lifetime in sample N80 is not accounted for in either PL or PCD measurements in which the actual minority carrier concentration varies as a function of depth, i.e., only a weighted averaged injection level [16] is considered. The PL and PCD measurements also make use of different measurement modes (steady-state versus transient), which would also produce different minority carrier profiles as a function of depth and time. Finally, misalignment of the location of PL and PCD measurements or the large difference in spatial averaging of the measurements could cause the observed discrepancies.

We conservatively estimate the total uncertainty of the PLIR lifetime method to be $\pm 30\%$, which is dominated by uncertainties in the individual modeling inputs (e.g., spectral sensitivities of the camera and filters) rather than experimental variances. Its value is of little dependence on injection level. We cannot quantify the total uncertainty of the PCD technique on thick samples but is likely to be lower than quasi-steady-state PC [26]. It is suspected that the trapping correction introduces an increasingly significant uncertainty toward lower injections reaching up to 50% uncertainty at an injection level one order of magnitude below the trap density, i.e., 50% uncertainty at $10^{13}\,\mathrm{cm}^{-3}$ for these samples based on guidance from the tool manufacturer (R. Sinton, personal communication). A $\pm$ 4% statistical repeatability has been reported for PCD lifetime measurements on bulk samples [27].

Despite having considerably lower lifetime, central parts of sample N80 emit a similar PL intensity compared to N674 in the sensitivity range of the camera, which is explained by higher effective doping. This is in contrast to the phosphorus doping profile predicted by the Scheil equation [28], according to which the doping concentration is expected to be lower near the crown/seed (N80) compared to positions further along the growth direction (N674). A possible explanation for the lower lifetime and higher effective doping in the center of sample N80 is an increased concentration of TD, which are common in the parts of the ingot closer to the seed that are solidified first [2]. One distinguishing feature of TDs is that they may be present in an ionized state, which simultaneously act as recombination sites and as donors, contributing up to two free electrons depending on the background doping and temperature [2].

Since PL intensity under low injection conditions is proportional to the effective doping concentration, a single PL image can be used together with bulk lifetime images to quantify the relative doping differences within and between discs [6]. Fig. 6 shows the relative doping of both discs, normalized to the maximum doping present in N80. The low lifetime region in N80 is correlated with a region of high effective doping. The lifetime improves toward the edges of N80, where the effective doping decreases, which can be seen in the cross-sectional profiles in Fig. 7. We observe good agreement between the relative doping values measured by PL and the dark conductance measurements from a Sinton BCT-400. Using Fourier transform infrared (FT-IR) spectrophotometry, we confirmed that the center of N80 has 1.4 times higher interstitial oxygen concentration ($[\mathrm{O}_i]$) than the center of N674, based on the absorption at 1720 cm^{-1} [29]. A series of FT-IR spot measurements also confirmed both samples had a gradual reduction in $[O_i]$ from the center toward the perimeter in a similar trend as seen in other studies on CZ-Si [30]. Since the presence of TDs is correlated with the interstitial oxygen concentration [31], these measurements qualitatively agree with the trends observed in the bulk lifetime and relative doping in these samples.

V. Conclusion

We have explored the sensitivity of the PLIR lifetime technique for different sample thicknesses and have shown that unpassivated samples with more than 4 mm thickness are required to reliably measure bulk lifetime on state-of-the-art n-type CZ Si. Lifetimes ranging from 0.8 to 20 ms were measured on unpassivated 20 mm thick n-type Si discs, highlighting the large variance present in state-of-the-art CZ production ingots especially near the crown. In applying the method to thick wafers rather than bricks, specific major defects of concern for CZ Si, likely related to oxygen, have been observed near the crown. Relative doping and absolute bulk lifetime values obtained from the PLIR method were demonstrated to be consistent with transient PC and resistivity measurements within the limitations of the transient PC-based technique.

ACKNOWLEDGMENT

The authors would like to acknowledge M. Juhl for assistance with modeling and R. Sinton and A. Blum for helpful discussions regarding photoconductance measurements and minority carrier trapping.

REFERENCES

[1] J. D. Murphy, R. E. McGuire, K. Bothe, V. V. Voronkov, and R. J. Falster, "Minority carrier lifetime in silicon photovoltaics: The effect of oxygen precipitation," *Sol. Energy Mater. Sol. Cells*, vol. 120, pp. 402–411, Jan. 2014.

[2] M. Tomassini *et al.*, "Recombination activity associated with thermal donor generation in monocrystalline silicon and effect on the conversion efficiency of heterojunction solar cells," *J. Appl. Phys.*, vol. 119, no. 8, Feb. 2016, Art. ID. 84508.

[3] S. De Wolf, A. Descoeudres, Z. C. Holman, and C. Ballif, "High-efficiency silicon heterojunction solar cells: A review," *Green*, vol. 2, no. 1, pp. 7–24, Jan. 2012.

[4] D. D. Smith *et al.*, "Toward the practical limits of silicon solar cells," *IEEE J. Photovolt.*, vol. 4, no. 6, pp. 1465–1469, Nov. 2014.

[5] J. S. Swirhun, R. A. Sinton, M. K. Forsyth, and T. Mankad, "Contactless measurement of minority carrier lifetime in silicon ingots and bricks," *Prog. Photovolt. Res. Appl.*, vol. 19, no. 3, pp. 313–319, 2011.

[6] B. Mitchell, T. Trupke, J. W. Weber, and J. Nyhus, "Bulk minority carrier lifetimes and doping of silicon bricks from photoluminescence intensity ratios," *J. Appl. Phys.*, vol. 109, no. 8, 2011, Art. ID. 83111.

[7] J. A. Giesecke, R. A. Sinton, M. C. Schubert, S. Riepe, and W. Warta, "Determination of bulk lifetime and surface recombination velocity of silicon ingots from dynamic photoluminescence," *IEEE J. Photovolt.*, vol. 3, no. 4, pp. 1311–1318, Oct. 2013.

[8] N. E. Grant, K. R. McIntosh, and J. T. Tan, "Evaluation of the bulk lifetime of silicon wafers by immersion in hydrofluoric acid and illumination," *ECS J. Solid State Sci. Technol.*, vol. 1, no. 2, pp. P55–P61, Jul. 2012.

[9] C. Schinke, D. Hinken, J. Schmidt, K. Bothe, and R. Brendel, "Modeling the spectral luminescence emission of silicon solar cells and wafers," *IEEE J. Photovolt.*, vol. 3, no. 3, pp. 1038–1052, Jul. 2013.

[10] M. A. Green, "Analytical expressions for spectral composition of band photoluminescence from silicon wafers and bricks," *Appl. Phys. Lett.*, vol. 99, no. 2011, pp. 147–150, 2011.

[11] H. Haug, J. Greulich, A. Kimmerle, and E. S. Marstein, "PC1Dmod 6.1—State-of-the-art models in a well-known interface for improved simulation of Si solar cells," *Sol. Energy Mater. Sol. Cells*, vol. 142, pp. 1–7, 2015.

[12] A. Schenk, "Finite-temperature full random-phase approximation model of band gap narrowing for silicon device simulation," *J. Appl. Phys.*, vol. 84, no. 7, p. 3684–3695, 1998.

[13] D. B. M. Klaassen, "A unified mobility model for device simulation—I. Model equations and concentration dependence," *Solid State Electron.*, vol. 35, no. 7, pp. 953–959, Jul. 1992.

[14] D. B. M. Klaassen, "A unified mobility model for device simulation—II. Temperature dependence of carrier mobility and lifetime," *Solid State Electron.*, vol. 35, no. 7, pp. 961–967, Jul. 1992.

[15] A. Richter, S. W. Glunz, F. Werner, J. Schmidt, and A. Cuevas, "Improved quantitative description of Auger recombination in crystalline silicon," *Phys. Rev. B*, vol. 86, no. 16, 2012, Art. ID. 165202.

[16] S. Bowden and R. A. Sinton, "Determining lifetime in silicon blocks and wafers with accurate expressions for carrier density," *J. Appl. Phys.*, vol. 102, no. 12, 2007, Art. ID. 124501.

[17] K. Bothe, R. Krain, R. Falster, and R. Sinton, "Determination of the bulk lifetime of bare multicrystalline silicon wafers," *Prog. Photovolt. Res. Appl.*, vol. 18, no. 3, pp. 204–208, 2010.

[18] J. A. Giesecke, M. Kasemann, and W. Warta, "Determination of local minority carrier diffusion lengths in crystalline silicon from luminescence images," *J. Appl. Phys.*, vol. 106, no. 1, 2009, Art. ID. 14907.

[19] B. Mitchell, D. Chung, and A. Teal, "Photoluminescence imaging using silicon line-scanning cameras," *IEEE J. Photovolt.*, vol. 6, no. 4, pp. 967–975, Jul. 2016.

[20] K. Youssef, M. Shi, C. Radue, E. Good, and G. Rozgonyi, "Effect of oxygen and associated residual stresses on the mechanical properties of high growth rate Czochralski silicon," *J. Appl. Phys.*, vol. 113, no. 13, 2013, Art. ID. 133502.

[21] B. Mitchell, J. Greulich, and T. Trupke, "Quantifying the effect of minority carrier diffusion and free carrier absorption on photoluminescence bulk lifetime imaging of silicon bricks," *Sol. Energy Mater. Sol. Cells*, vol. 107, pp. 75–80, 2012.

[22] S. P. Phang, H. C. Sio, and D. Macdonald, "Applications of carrier desmearing of photoluminescence images on silicon wafers," *Prog. Photovolt. Res. Appl.*, vol. 24, no. 12, pp. 1547–1553, 2016.

[23] J. R. Haynes and J. A. Hornbeck, "Trapping of minority carriers in silicon. II. n-type silicon," *Phys. Rev.*, vol. 100, no. 2, pp. 606–615, Oct. 1955.

[24] Y. Hu, H. Schøn, O. Nielsen, E. J. Ovrelid, and L. Arnberg, "Investigating minority carrier trapping in n-type Cz silicon by transient photoconductance measurements," *J. Appl. Phys.*, vol. 111, no. 5, 2012, Art. ID. 53101.

[25] R. A. Bardos, T. Trupke, M. C. Schubert, and T. Roth, "Trapping artifacts in quasi-steady-state photoluminescence and photoconductance lifetime measurements on silicon wafers," *Appl. Phys. Lett.*, vol. 88, no. 5, pp. 1–3, 2006.

[26] K. R. McIntosh and R. A. Sinton, "Uncertainty in photoconductance lifetime measurements that use an inductive-coil detector," in *Proc. 23rd Eur. Photovolt. Sol. Energy Conf. Exhib.*, 2008, pp. 77–82.

[27] A. L. Blum *et al.*, "Inter-laboratory study of eddy-current measurement of excess-carrier recombination lifetime," in *Proc. IEEE Photovolt. Spec. Conf.*, 2013, pp. 1396–1401.

[28] E. Scheil, "Bemerkungen zur Schichtkristallbildung," *Z. Met.*, vol. 34, no. 3, pp. 70–72, 1942.

[29] B. Pajot, H. J. Stein, B. Cales, and C. Naud, "Quantitative spectroscopy of interstitial oxygen in silicon," *J. Electrochem. Soc.*, vol. 132, no. 12, pp. 3034–3037, 1985.

[30] S. Y. Lim, F. E. Rougieux, and D. Macdonald, "Boron-oxygen defect imaging in p-type Czochralski silicon," *Appl. Phys. Lett.*, vol. 103, no. 9, 2013, Art. ID. 92105.

[31] W. Kaiser, H. L. Frisch, and H. Reiss, "Mechanism of the formation of donor states in heat-treated silicon," *Phys. Rev.*, vol. 112, no. 5, pp. 1546–1554, 1958.

Authors' photographs and biographies not available at the time of publication.